

# Negative-parity high-spin states and a possible magnetic rotation band in $^{135}\text{Pr}_{76}$

Ritika Garg,<sup>1,2,\*</sup> S. Kumar,<sup>1</sup> Mansi Saxena,<sup>1</sup> Savi Goyal,<sup>1</sup> Davinder Siwal,<sup>1</sup> Sunil Kalkal,<sup>3</sup> S. Verma,<sup>1</sup> R. Singh,<sup>4</sup> S. C. Pancholi,<sup>2</sup> R. Palit,<sup>5</sup> Deepika Choudhury,<sup>6</sup> S. S. Ghugre,<sup>7</sup> G. Mukherjee,<sup>8</sup> R. Kumar,<sup>2</sup> R. P. Singh,<sup>2</sup> S. Muralithar,<sup>2</sup> R. K. Bhownik,<sup>2</sup> and S. Mandal<sup>1</sup>

<sup>1</sup>Department of Physics and Astrophysics, University of Delhi, Delhi 110007, India

<sup>2</sup>Inter University Accelerator Centre, Aruna Asif Ali Marg, New Delhi 110067, India

<sup>3</sup>Department of Nuclear Physics, Australian National University, Canberra, Australian Capital Territory 0200, Australia

<sup>4</sup>AINST, Amity University, Noida, India

<sup>5</sup>Department of Nuclear and Atomic Physics, Tata Institute of Fundamental Research, Mumbai 400005, India

<sup>6</sup>ELI-NP, Hora Hulubei National Institute of Physics and Nuclear Engineering, 077125 Magurele, Romania

<sup>7</sup>UGC -DAE Consortium for Scientific Research, Kolkata 700098, India

<sup>8</sup>Physics Group, Variable Energy Cyclotron Centre, Kolkata 700064, India

(Received 26 August 2015; published 30 November 2015)

Excited states in  $^{135}\text{Pr}$  have been investigated using the reaction  $^{123}\text{Sb}(^{16}\text{O}, 4n)^{135}\text{Pr}$  at an incident beam energy of 82 MeV. The partial level scheme has been established for negative-parity states with addition of new  $\gamma$ -ray transitions. The directional correlation and polarization measurements have been performed to assign spin parity for most of the reported  $\gamma$ -ray transitions. At high spin, a negative-parity dipole band ( $\Delta I = 1$ ) has been reported along with the observation of new crossover  $E2$  transitions. Tilted Axis Cranking (TAC) calculations have been performed by considering a three-quasiparticle (3qp) configuration  $\pi(h_{11/2})^1 \otimes \nu(h_{11/2})^{-2}$  and a five-quasiparticle (5qp) configuration  $\pi(h_{11/2})^1(g_{7/2})^2 \otimes \nu(h_{11/2})^{-2}$  for the lower and upper parts of the band, respectively. The observed results are compared with the results of the theoretical (TAC) calculations.

DOI: [10.1103/PhysRevC.92.054325](https://doi.org/10.1103/PhysRevC.92.054325)

PACS number(s): 21.10.Hw, 21.60.Ev, 23.20.Lv, 27.60.+j

## I. INTRODUCTION

Nuclei in the mass region  $A \sim 135$  have been studied to investigate high-spin phenomena, e.g., superdeformation, chirality, and magnetic rotation (MR) [1–3]. Several decoupled bands based on  $\pi h_{11/2}$  orbital have been identified across odd- $Z$  nuclei in this mass region [4,5]. The opposite deformation-driving tendencies of neutron and proton quasiparticles in  $h_{11/2}$  subshell makes this region interesting to study shape-driving effects of specific valence particles. Particularly, across  $Z = 59$  odd- $A$  nuclei, rotational bands built on negative-parity states have been interpreted as arising from  $h_{11/2}$  proton orbitals and positive-parity states from  $g_{7/2}$ ,  $d_{5/2}$  proton orbitals [6–11]. In  $^{133}\text{Pr}$  and  $^{137}\text{Pr}$  nuclei, high-spin negative-parity  $\Delta I = 1$  band structures have been interpreted as arising from a pair of rotationally aligned  $h_{11/2}$  protons and  $h_{11/2}$  neutrons orbitals. These bands, consisting of strong magnetic dipole transitions, have been identified as MR bands [12,13]. Moreover, in  $^{137}\text{Pr}$ , MR band crossing has also been observed. In the  $^{135}\text{Pr}$  isotope, a band structure similar to the above-mentioned  $\Delta I = 1$  band was tentatively reported [8]. However, there has been no detailed study on this band.

The present experimental work is focused to explore this band structure for MR and MR band crossing in  $^{135}\text{Pr}$ . The  $^{135}\text{Pr}$  nucleus has been previously studied by using the  $^{136}\text{Ce}(^{11}\text{B}, 4n)$ ,  $^{120}\text{Sn}(^{19}\text{F}, 4n)$ ,  $^{123}\text{Sb}(^{16}\text{O}, 4n)$ , and  $^{116}\text{Cd}(^{23}\text{Na}, 4n)$  reactions [8,9,14,15] apart from the  $\beta$  decay of  $^{135}\text{Nd}$  [16]. Several theoretical studies have been carried out to understand the low-spin positive- and negative-parity

band structures [5,17–21]. Recently, the phenomenon of transverse wobbling has been investigated in  $^{135}\text{Pr}$  [22]. In the present work, the negative-parity level structure of  $^{135}\text{Pr}$  has been discussed with experimental results and theoretical interpretation using Tilted Axis Cranking (TAC) calculations in the framework of hybrid model [23].

## II. EXPERIMENTAL DETAILS

High-spin states in  $^{135}\text{Pr}$  were populated by the reaction  $^{123}\text{Sb}(^{16}\text{O}, 4n)^{135}\text{Pr}$  using a  $^{16}\text{O}$  beam of 82 MeV from the pelletron accelerator at the Inter University Accelerator Centre (IUAC), New Delhi [24,25]. The target consisted of a  $800 \mu\text{g}/\text{cm}^2$   $^{123}\text{Sb}$  with  $10 \text{ mg}/\text{cm}^2$   $^{197}\text{Au}$  backing. The deexciting  $\gamma$  rays were detected using the Indian National Gamma Array (INGA) [26,27]. At the time of the experiment, the array consisted of 15 Compton-suppressed clover high-purity germanium detectors placed at  $32^\circ$ ,  $57^\circ$ ,  $90^\circ$ ,  $123^\circ$ , and  $148^\circ$  with three, two, four, two, and four detectors, respectively. The detectors were placed at a distance of 25 cm from the target. The list mode data were taken in triple and higher fold  $\gamma$ -ray coincidence using a computer automated measurement and control based multiparameter data-acquisition system along with the Collection and Analysis of Nuclear Data using Linux nEtwork (CANDLE) [28] software. A total of about  $300 \times 10^6$  events were recorded in the experiment. The data were sorted using the INGASORT [29] program and the coincidence events were sorted to produce symmetric and asymmetric matrices. The RADWARE software package was used to analyze the coincidence matrices [30]. The multipolarities of the  $\gamma$ -ray transitions were extracted by using the asymmetric angle-dependent matrix with the events

\* ritikagarg25@gmail.com

TABLE I. Level energy  $E_i$ ,  $\gamma$  energy  $E_\gamma$ , relative intensity  $I_\gamma$ ,  $R_{DCO}$ , polarization asymmetry  $\Delta$ , multipolarity, and decay from initial spin  $J_i^\pi$  to final spin  $J_f^\pi$  for the  $\gamma$ -ray transitions in  $^{135}\text{Pr}$ . Superscripts Q and D stand for the quadrupole and dipole nature of the gating transition in the determination of  $R_{DCO}$ . Uncertainty in  $E_\gamma$  is  $\pm 0.2$  and  $\pm 0.5$  keV for strong and weak  $\gamma$ -ray transitions, respectively.

$E_i$ (keV)	$E_\gamma$ (keV)	$I_\gamma$ (rel.)	$R_{DCO}$	$\Delta$	Multipolarity	$J_i^\pi \rightarrow J_f^\pi$
3530.0	149.5	1.13(5)	0.50(4) <sup>Q</sup>		D	$27/2^- \rightarrow 25/2^{(-)}$
5028.6	325.1	10.83(25)	1.28(5) <sup>D</sup>	-0.12(0.06)	$M1$	$35/2^- \rightarrow 33/2^-$
3863.0	332.9	13.1(3)	0.47(3) <sup>Q</sup>	-0.03(0.08)	$M1$	$29/2^- \rightarrow 27/2^-$
3863.0	345.2	2.20(10)	0.36(5) <sup>Q</sup>		D	$29/2^- \rightarrow 27/2^{(-)}$
730.9	372.8	100.0(18)	1.00(2) <sup>Q</sup>	0.08(0.04)	$E2$	$15/2^- \rightarrow 11/2^-$
3863.0	375.9	2.29(23)	0.48(4) <sup>Q</sup>		D	$29/2^- \rightarrow 27/2^-$
4704.1	383.9	1.71(8)	0.37(8) <sup>Q</sup>		D	$33/2^- \rightarrow 31/2^-$
4704.1	410.8	7.60(24)	0.51(7) <sup>Q</sup>	-0.16(0.10)	$M1$	$33/2^- \rightarrow 31/2^-$
2617.3	412.9	2.28(12)				$23/2^- \rightarrow 21/2^-$
5452.6	424.0	4.80(13)	0.33(4) <sup>Q</sup>	-0.15(0.09)	$M1$	$37/2^- \rightarrow 35/2^-$
4292.7	429.7	11.0(3)	0.45(3) <sup>Q</sup>	-0.05(0.06)	$M1$	$31/2^- \rightarrow 29/2^-$
1928.4	450.0	3.53(12)	0.34(2) <sup>Q</sup>		D	$19/2^- \rightarrow 17/2^-$
3380.6	469.8	0.26(7)				$25/2^{(-)} \rightarrow (25/2^-)$
1433.5	481.7	2.78(6)				$(17/2^-) \rightarrow 13/2^-$
1928.4	494.9	0.99(5)	1.58(61) <sup>Q</sup>		$D+Q$	$19/2^- \rightarrow (17/2^-)$
5951.1	498.5	4.88(16)	0.83(4) <sup>D</sup>	-0.14(0.07)	$M1$	$39/2^- \rightarrow 37/2^-$
1478.2	526.4	0.82(5)				$17/2^- \rightarrow 13/2^-$
6506.4	555.3	1.7(2)	0.87(14) <sup>D</sup>		D	$41/2^{(-)} \rightarrow 39/2^-$
951.8	593.7		0.72(7) <sup>Q</sup>	-0.13(0.12)	$M1$	$13/2^- \rightarrow 11/2^-$
2754.8	595.8					$23/2^- \rightarrow (21/2^-)$
7110.4	604.0					$(43/2^-) \rightarrow 41/2^{(-)}$
1391.1	660.2	84.3(15)	0.98(2) <sup>Q</sup>	0.06(0.03)	$E2$	$19/2^- \rightarrow 15/2^-$
2910.8	665.7	0.9(3)				$(25/2^-) \rightarrow 23/2^-$
2617.3	688.8	5.96(17)	1.36(11) <sup>Q</sup>	0.07(0.06)	$E2$	$23/2^- \rightarrow 19/2^-$
2158.9	725.4	0.87(6)				$(21/2^-) \rightarrow (17/2^-)$
2204.4	726.0	3.59(16)				$21/2^- \rightarrow 17/2^-$
5028.6	735.9	0.50(3)				$35/2^- \rightarrow 31/2^-$
1478.2	747.5	9.06(24)	0.25(1) <sup>Q</sup>	-0.05(0.03)	$M1 + E2$	$17/2^- \rightarrow 15/2^-$
3000.4	755.3	1.83(15)	0.46(4) <sup>Q</sup>		D	$25/2^{(-)} \rightarrow 23/2^-$
4292.7	762.7	1.58(8)				$31/2^- \rightarrow 27/2^-$
3519.0	764.2	4.81(18)	2.13(37) <sup>D</sup>		Q	$27/2^{(-)} \rightarrow 23/2^-$
2158.9	767.9	1.02(8)				$(21/2^-) \rightarrow 19/2^-$
3530.0	776.2	7.75(23)	0.83(6) <sup>Q</sup>	0.15(12)	$E2$	$27/2^- \rightarrow 23/2^-$
3000.4	795.9	4.43(15)	0.98(10) <sup>Q</sup>		Q	$25/2^{(-)} \rightarrow 21/2^-$
2204.4	813.3	5.96(18)	0.22(2) <sup>Q</sup>	-0.2(0.08)	$M1 + E2$	$21/2^- \rightarrow 19/2^-$
2754.8	826.3	1.85(10)	1.08(13) <sup>Q</sup>		Q	$23/2^- \rightarrow 19/2^-$
5998.0	834.0	3.65(14)	0.97(16) <sup>Q</sup>	0.24(0.14)	$E2$	$39/2^- \rightarrow 35/2^{(-)}$
4704.1	840.6	1.63(7)				$33/2^- \rightarrow 29/2^-$
5164.0	843.8	3.39(13)	0.84(10) <sup>Q</sup>		Q	$35/2^{(-)} \rightarrow 31/2^-$
2245.1	854.0	42.4(11)	0.98(11) <sup>Q</sup>	0.09(0.06)	$E2$	$23/2^- \rightarrow 19/2^-$
3487.9	870.8	7.2(7)	0.98(8) <sup>Q</sup>	0.12(0.10)	$E2$	$27/2^- \rightarrow 23/2^-$
6879.2	881.2	2.10(7)	0.79(14) <sup>Q</sup>		Q	$43/2^{(-)} \rightarrow 39/2^-$
3530.0	913.6	1.45(16)	2.11(19) <sup>D</sup>		Q	$27/2^- \rightarrow 23/2^-$
7801.8	922.6	1.29(7)	1.33(16) <sup>Q</sup>		Q	$47/2^{(-)} \rightarrow 43/2^{(-)}$
3955.6	955.2	3.99(18)	1.00(9) <sup>Q</sup>		Q	$29/2^{(-)} \rightarrow 25/2^{(-)}$
8757.8	956.0					$(51/2^-) \rightarrow 47/2^{(-)}$
3245.0	999.9	13.1(4)	0.95(5) <sup>Q</sup>	0.12(0.06)	$E2$	$27/2^- \rightarrow 23/2^-$
4292.7	1048.5	3.04(13)	1.27(13) <sup>Q</sup>		Q	$31/2^- \rightarrow 27/2^-$
4320.2	1075.2	6.90(20)	0.94(8) <sup>Q</sup>	0.22(0.12)	$E2$	$31/2^- \rightarrow 27/2^-$
5068.1	1112.5					$(33/2^-) \rightarrow 29/2^{(-)}$
4394.2	1149.2	1.57(10)	0.49(4) <sup>Q</sup>		D	$29/2^{(-)} \rightarrow 27/2^-$
1928.4	1197.4	5.08(23)	0.84(7) <sup>Q</sup>	0.12(0.11)	$E2$	$19/2^- \rightarrow 15/2^-$
2617.3	1225.9	5.8(3)	0.87(6) <sup>Q</sup>	0.11(0.07)	$E2$	$23/2^- \rightarrow 19/2^-$
3519.0	1273.5	0.61(7)	0.78(14) <sup>Q</sup>		Q	$27/2^{(-)} \rightarrow 23/2^-$
3530.0	1285.7	2.86(12)	0.90(8) <sup>Q</sup>		Q	$27/2^- \rightarrow 23/2^-$
2754.8	1363.7	5.38(10)	0.71(4) <sup>Q</sup>	0.09(0.05)	$E2$	$23/2^- \rightarrow 19/2^-$

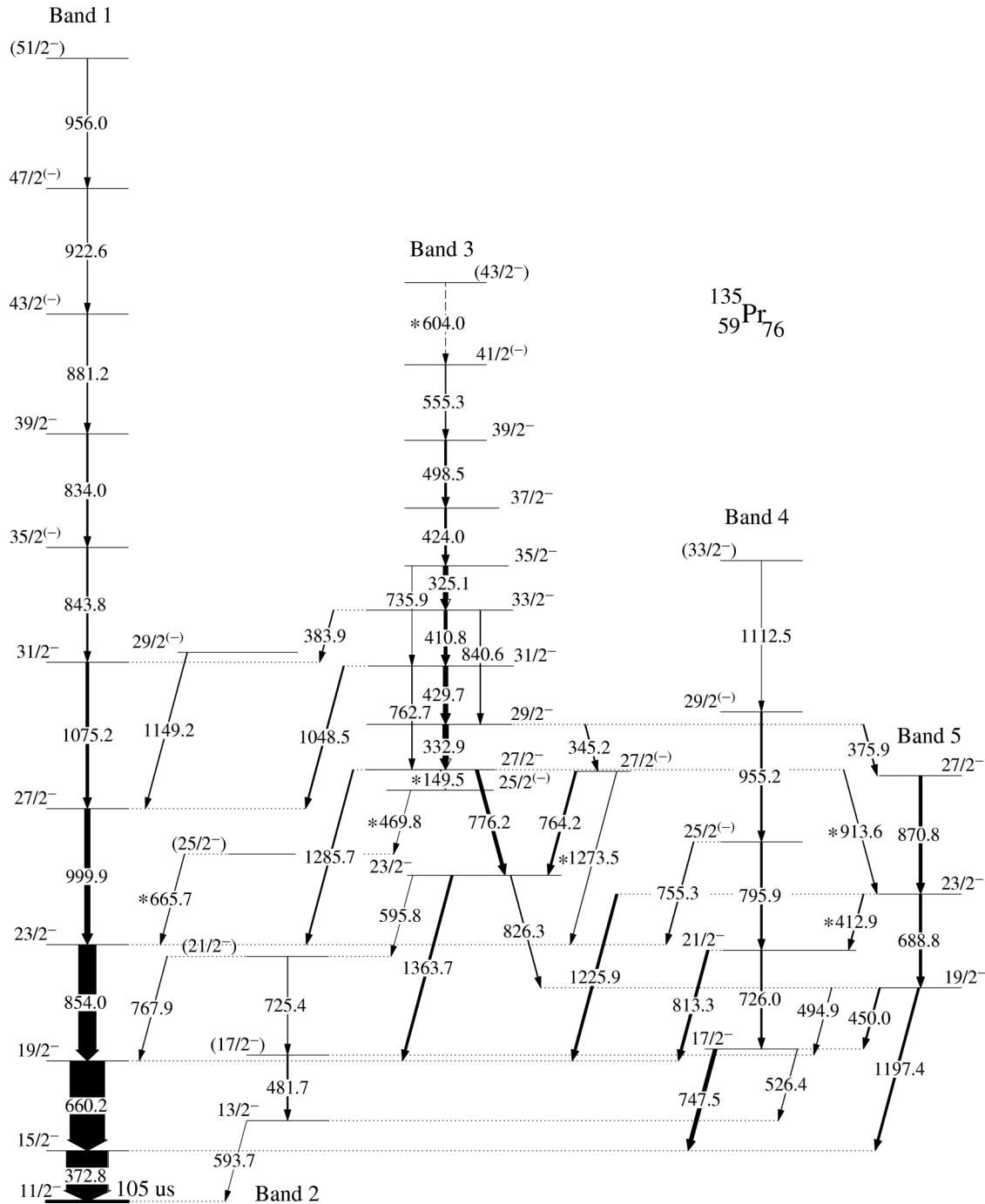


FIG. 1. The partial level scheme of  $^{135}\text{Pr}$  deduced from the present work. New transitions are marked with an asterisk (\*).

detected by clovers at  $90^\circ$  on one axis and by clovers at  $148^\circ$  on the other axis. The Directional Correlations of Oriented states (DCO) ratios were calculated using the following relation:

$$R_{\text{DCO}} = \frac{I_{148^\circ}^{\gamma_2}(\text{Gate}_{90^\circ}^{\gamma_1})}{I_{90^\circ}^{\gamma_2}(\text{Gate}_{148^\circ}^{\gamma_1})}. \quad (1)$$

The DCO ratios for a particular  $\gamma$ -ray transition were obtained by setting gates on known stretched quadrupole and dipole transitions. The DCO ratios obtained with a stretched quadrupole gate are  $\sim 1$  for stretched quadrupole and  $\sim 0.4$  for

dipole transitions. The ratio is close to 0.8 for a dipole and 2.0 for a quadrupole transition when the gate is set on a dipole transition. The linear polarization measurements of  $\gamma$ -ray transitions were done for the first time in this nucleus using the Integrated Polarizational Directional Correlation (IPDCO) method [31]. In this method, the experimental polarization asymmetry factor of Compton-scattered polarized photons is defined as

$$\Delta = \frac{a(E_\gamma)N_\perp - N_\parallel}{a(E_\gamma)N_\perp + N_\parallel}, \quad (2)$$

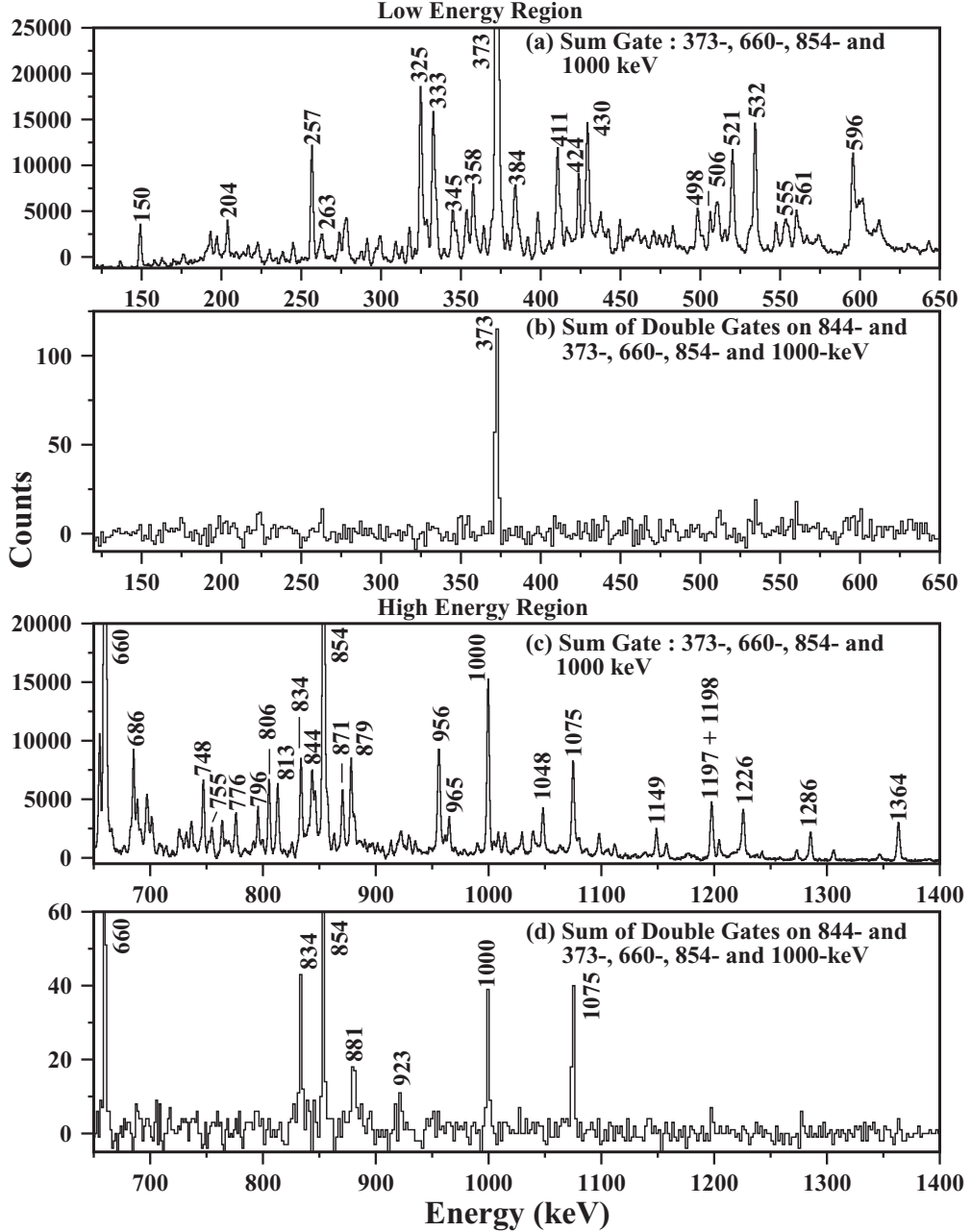


FIG. 2. (a),(c) Sum of gated  $\gamma$ - $\gamma$  coincidence spectra. (b),(d) Sum of double-gated spectrum with 844 keV and 373, 660, 854, and 1000 keV (see text for explanation).

where  $N_{\perp}$  ( $N_{\parallel}$ ) denote the number of counts of  $\gamma$ -ray transitions scattered perpendicular (parallel) to the reaction plane within a clover detector [32]. The correction factor  $a(E_{\gamma})$  denotes the correction owing to the asymmetry in response of the perpendicular and parallel clover segments. This factor was obtained from the analysis of the single  $\gamma$  rays emitted by  $^{152}\text{Eu}$  source placed at the target position and defined as

$$a(E_{\gamma}) = \frac{N_{\parallel}(\text{unpolarized})}{N_{\perp}(\text{unpolarized})}. \quad (3)$$

The value of  $a(E_{\gamma})$  was found to be about 0.93(6). The experimental asymmetry,  $\Delta$ , was evaluated by generating two asymmetric matrices. These matrices contained events with one axis corresponding to perpendicular or parallel scattered events in the detectors at  $90^\circ$  and another axis corresponding to all the detectors of the array. Gates were set on the latter axis to get polarization asymmetry ( $\Delta$ ) from the intensity of coincident perpendicular or parallel scattered  $\gamma$  rays using Eq. (2). A positive value of  $\Delta$  is indicative of electric character and a negative value indicates magnetic character of  $\gamma$ -ray transitions. The experimental values of  $\Delta$  obtained for various  $\gamma$ -ray transitions are given in Table I.

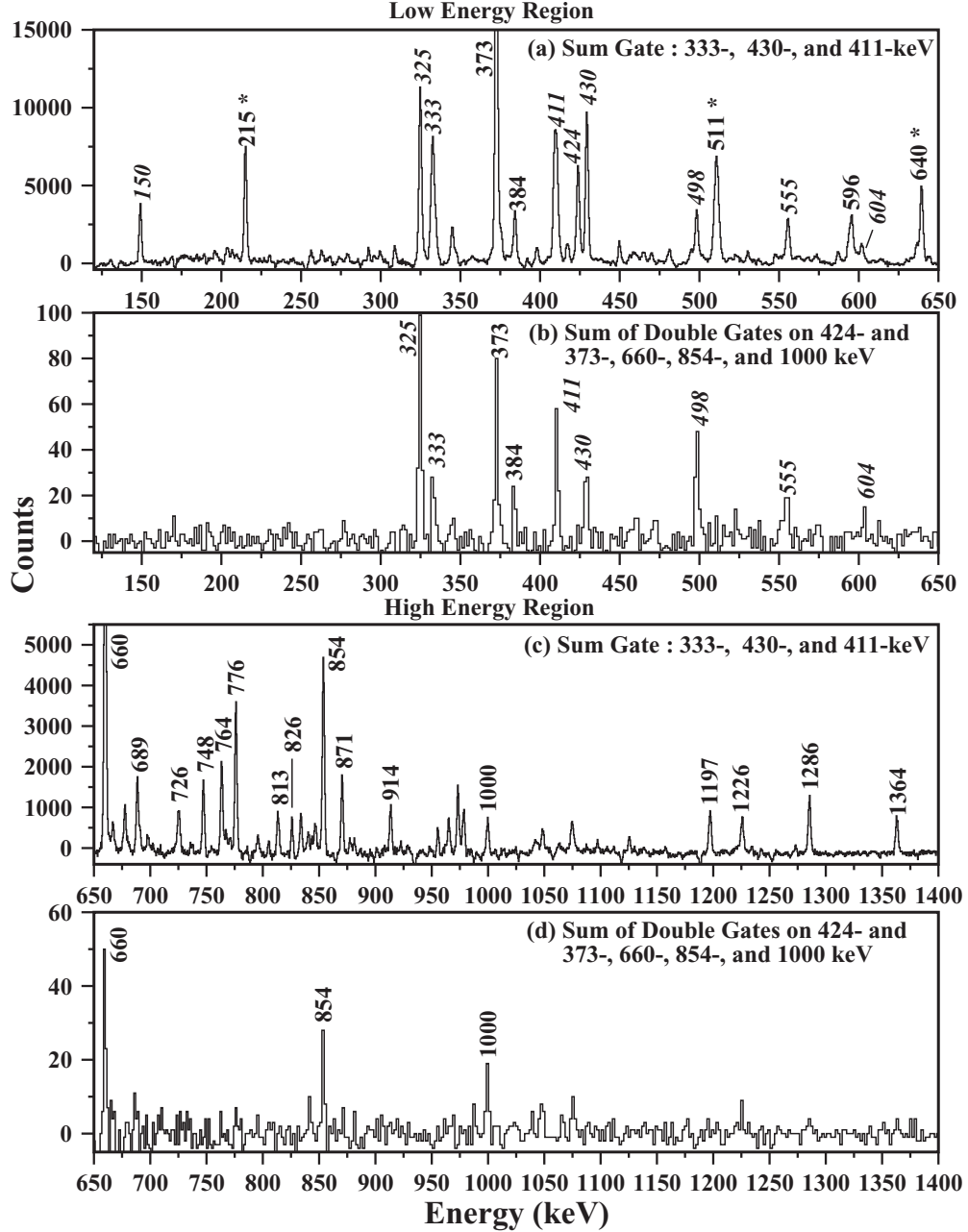


FIG. 3. (a),(c) Sum of gated  $\gamma$ - $\gamma$  coincidence spectra. (b),(d) Sum of double-gated spectrum with 424 keV and 373, 660, 854, and 1000 keV. (Transitions belonging to band 3 are marked in italics in all the spectra). The contaminant transitions are marked with an asterisk (\*).

### III. RESULTS AND DISCUSSION

The partial level scheme of  $^{135}\text{Pr}$  consisting of only the negative-parity states, from the present work, is shown in Fig. 1. It was constructed on the basis of  $\gamma$ - $\gamma$  and  $\gamma$ - $\gamma$ - $\gamma$  coincidence relationships and intensity considerations. Several new transitions have been identified and placed in this level scheme. The  $\gamma$ -ray transition energies, their relative intensities,  $R_{\text{DCO}}$ , and linear polarization asymmetry values, as obtained from the present work, are listed in Table I. The intensities have been calculated from the total projection as well as by the gated coincidence spectra normalized with respect to 373-keV transition. The various bands obtained are labeled bands 1–5, as shown in Fig. 1.

#### A. Band 1

The  $^{135}\text{Pr}$  ground-state spin and parity is  $3/2^+$ , the spin has been measured as  $3/2$  [33], and the parity is from systematics [16]. Band 1 is the yrast band based on an isomeric state at 358 keV having a half-life of  $105 \mu\text{s}$  and spin  $11/2^-$  [34]. This band has been identified as a decoupled band [16]. On the basis of lifetime measurements for the low-lying levels in band 1, the decrease in their quadrupole moments with frequency was attributed owing to change in deformation [14]. This band consists of 373-, 660-, 854-, 1000-, 1075-, 844-, 834-, 881-, 923-, and 956-keV transitions. In Ref. [15], it has been observed to very high spins ( $J^\pi = 91/2^-$ ) with ten transitions above the 956-keV transition. The emphasis

of our work is on the  $R_{DCO}$  and polarization measurements of the observed  $\gamma$  rays in this band. On the basis of our  $R_{DCO}$  and  $\Delta$  value measurements, the transitions 373-, 660-, 854-, 1000-, 1075-, and 834-keV have been assigned the multipolarity as  $E2$ . The spectrum displaying the transitions of this band is shown in Fig. 2.  $\gamma$  rays feeding into the yrast band from positive-parity and negative-parity bands are not seen in Figs. 2(b) and 2(d) because the 844-keV transition is above the feeding transition of negative-parity band 3 and positive-parity bands.

### B. Bands 2, 4, and 5

Band 2 consists of 482- and 725-keV transitions. It decays to the  $11/2^-$  and  $19/2^-$  states of band 1 via 593.7- and 767.9-keV transitions, respectively. This band has been identified as a signature partner band [22]. In our present work two interlinking transitions of 593.7 and 767.9 keV have been observed. The experimental  $R_{DCO}$  and polarization asymmetry values establish  $M1$  character for the 593.7-keV transition. Band 4 consists of 726-, 796-, 955-, and 1112-keV transitions. This band feeds band 1 through 748-, 813-, and 755-keV transitions at  $15/2^-$ ,  $19/2^-$ , and  $23/2^-$  levels, respectively. Recently, this band has been identified as a wobbler band [22]. Based on our linear polarization and  $R_{DCO}$  measurements the interconnecting transitions between bands 1 and 4, viz. of 748 and 813 keV, have been assigned as  $M1 + E2$  in nature. On the basis of the  $R_{DCO}$  measurement, it is found that another interlinking transition of 755 keV is dipole. Band 5 consists of 689- and 871-keV transitions. From our observed DCO ratios and  $\Delta$  values, the in-band transitions of band 5 are electric quadrupole ( $E2$ ).

### C. Band 3

Band 3 consists of 150-, 333-, 430-, 411-, 325-, 424-, 498-, and 555-keV transitions, along with a tentative placement of a 604-keV transition extending the excitation energy to 7110 keV. Figures 3(b) and 3(d) show the coincidence spectra obtained from the sum of double-gated spectra gated on 424

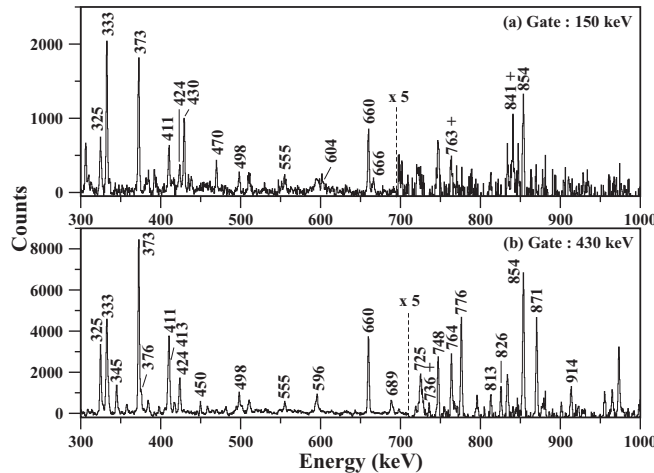


FIG. 4. Coincidence spectra showing the crossover transitions in band 3 (marked with a “+” sign).

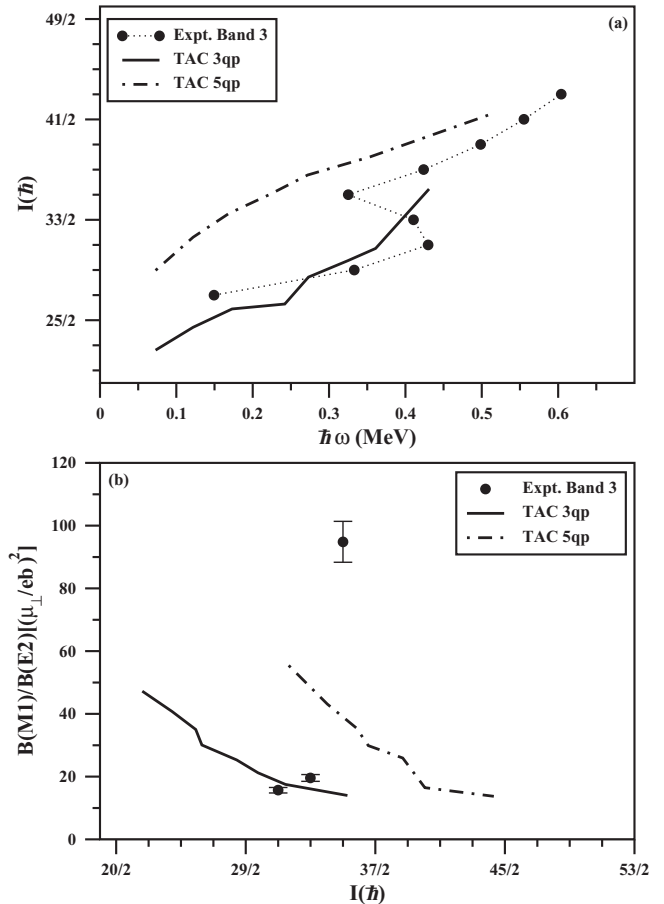


FIG. 5. (a) Comparison of the  $I(\hbar)$  vs  $\hbar\omega$  behavior with TAC calculations. (b) Experimental and calculated  $B(M1)/B(E2)$  ratios as functions of  $I(\hbar)$  for band 3.

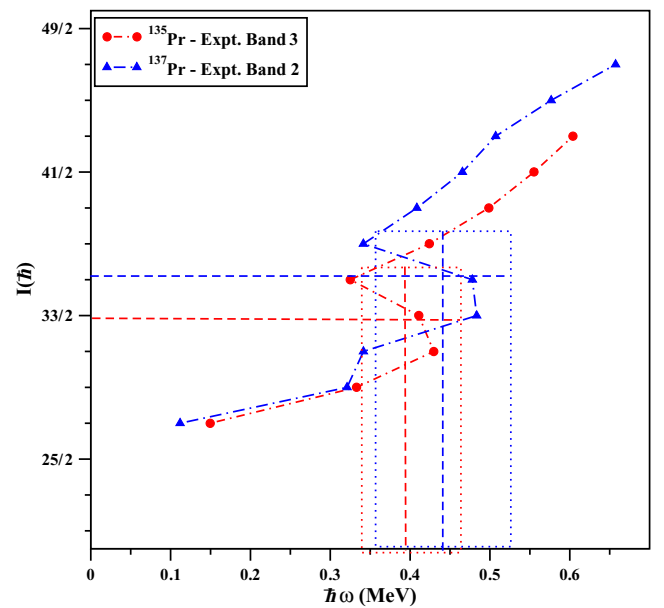


FIG. 6. (Color online)  $I(\hbar)$  vs  $\hbar\omega$  behavior of dipole bands in  $^{135}\text{Pr}$  and  $^{137}\text{Pr}$ .

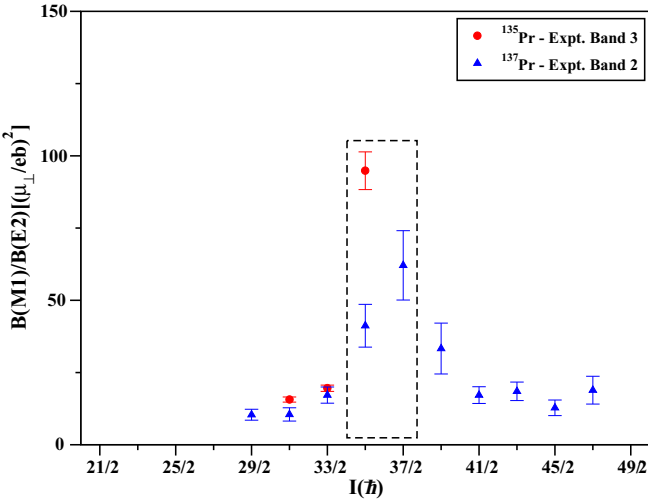


FIG. 7. (Color online) Variation of observed  $B(M1)/B(E2)$  ratios as functions of  $I(\hbar)$  for dipole bands in  $^{135}\text{Pr}$  and  $^{137}\text{Pr}$ .

and 373, 660, 854, 1000 keV. It shows that the low-lying transitions in band 1 are in coincidence with 424 keV belonging to band 3. The spectra show various transitions belonging to band 3. Figures 3(a) and 3(c) show the coincidence spectra obtained from the sum gating on the transitions 333, 430, and 411 keV. It shows transitions of band 3 and interconnecting transitions with other lower-lying levels. The  $R_{\text{DCO}}$  and polarization value of the 776-keV transition establishes it as an  $E2$  transition. The spin and parity of the energy level at 3531 keV is then  $I = 27/2^-$ . The transition of 150 keV which depopulates this level has been identified and placed

for the first time in the level scheme. This transition has been placed as the lowest transition in band 3. Our observed DCO ratio suggests that this transition is dipole. The  $R_{\text{DCO}}$  and polarization measurements for the 333-, 430-, 411-, 325-, 424-, and 498-keV transitions establish  $M1$  character for these transitions. Thus, band 3 has been identified as a negative-parity  $\Delta I = 1$  band. Figure 4 shows the crossover transitions of 736, 763, and 841 keV, which have been observed for the first time. In the present work, no lifetime was observed owing to the light ion beam and we are not able to extract  $B(M1)$  values for the energy levels of this band.

The TAC calculations were performed for band 3 using the hybrid version of the model as given in Ref. [23]. On the basis of systematics in this mass region, a three-quasiparticle (3qp) configuration  $\pi(h_{11/2})^1 \otimes \nu(h_{11/2})^{-2}$  and a 5qp configuration  $\pi(h_{11/2})^1(g_{7/2})^2 \otimes \nu(h_{11/2})^{-2}$  were used for the lower and upper parts of the band, respectively. For the TAC calculations, the pairing gap parameters were chosen to be 80% of the experimental even-odd mass difference, i.e.,  $\Delta_p = 1.08$  MeV and  $\Delta_n = 0.764$  MeV. The minimum in the total energy was obtained at  $\epsilon_2 = 0.14$ ,  $\gamma = 62^\circ$  with an average tilt angle  $\theta = 31.6^\circ$  for the 3qp configuration and at  $\epsilon_2 = 0.14$ ,  $\gamma = 60^\circ$  with an average tilt angle  $\theta = 26.9^\circ$  for the 5qp configuration, respectively. Figure 5(a) shows a comparison of the experimental behavior of spin  $I(\hbar)$  versus  $\hbar\omega$  with the TAC calculations and depicts a band crossing occurring at  $\hbar\omega \approx 0.37$  MeV. The results of our calculations show a good agreement with the experimental data in Fig. 5(a). The experimental  $B(M1)/B(E2)$  ratios for band 3 are shown in Fig. 5(b) along with the theoretical calculations. The  $B(M1)/B(E2)$  ratios as a function of spin show an increase with increase in spin up to  $I \approx 35/2^- \hbar$ . At higher spins,

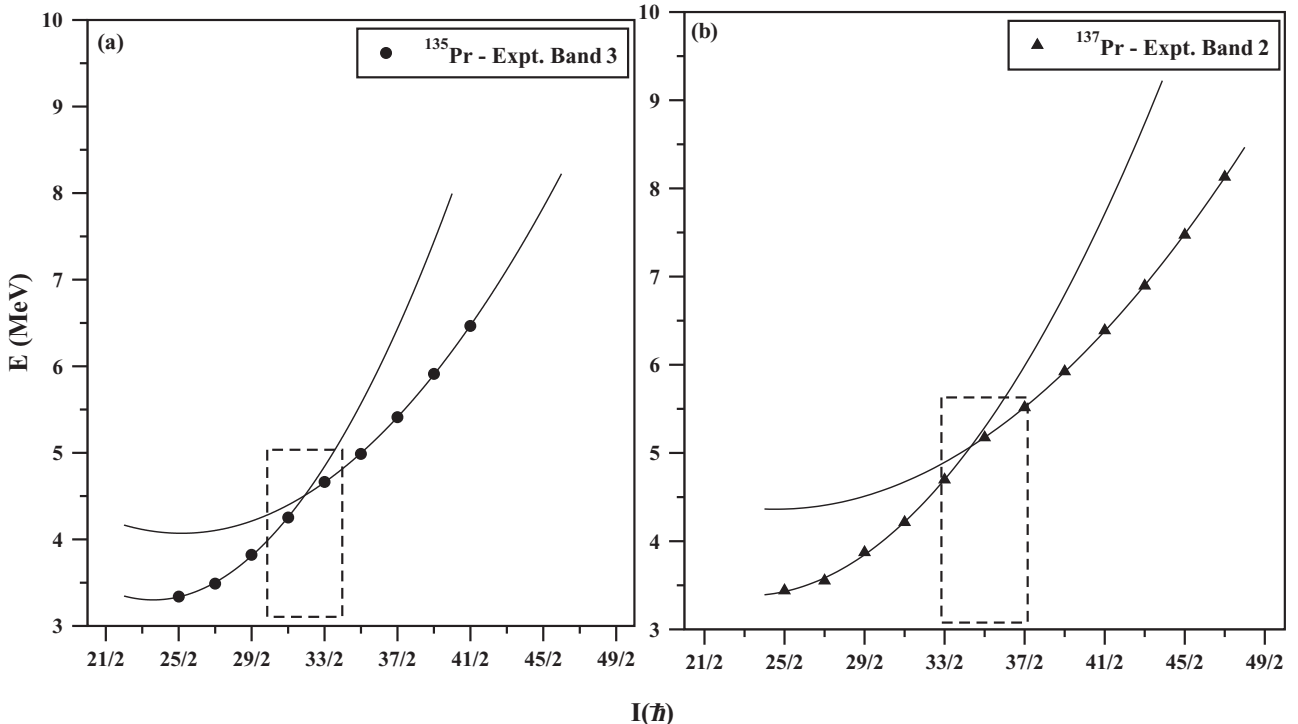


FIG. 8. Experimental energy vs spin  $I(\hbar)$  for dipole bands in  $^{135}\text{Pr}$  and  $^{137}\text{Pr}$ . The fitted lines are guides for seeing the band crossings.

the crossover transitions could not be observed owing to which  $B(M1)/B(E2)$  ratios could not be determined post band crossing behavior. Hence, the interpretation of the above band crossing from the behavior of  $B(M1)/B(E2)$  ratios is not possible.

The behavior of  $I(\hbar)$  versus  $\hbar\omega$  in  $^{135}\text{Pr}$  and  $^{137}\text{Pr}$  nuclei is similar except for the crossing spin and frequency. In  $^{135}\text{Pr}$ , crossing frequency and spin are  $\approx 0.37$  MeV,  $\approx 33/2^-$  as compared to  $\approx 0.42$  MeV,  $\approx 35/2^-$  in  $^{137}\text{Pr}$  (see Fig. 6). The comparison of  $B(M1)/B(E2)$  ratios versus  $I$  as well as  $E$  versus  $I$  both for  $^{135}\text{Pr}$  and  $^{137}\text{Pr}$  as shown in Figs. 7 and 8 also support the different crossing spin.

In brief, the  $^{135}\text{Pr}$  nucleus shows band crossing in the dipole band having a 3qp configuration  $[\pi(h_{11/2})^1 \otimes \nu(h_{11/2})^{-2}]$  for the lower part and 5qp configuration  $[\pi(h_{11/2})^1(g_{7/2})^2 \otimes \nu(h_{11/2})^{-2}]$  for the upper part, respectively. However the difference in crossing frequency and spin with respect to  $^{137}\text{Pr}$  may be attributable to the occupation of neutrons in different  $\Omega$  of the  $h_{11/2}$  Nilsson orbital.

#### IV. SUMMARY AND CONCLUSION

In summary, the negative-parity level structure of  $^{135}\text{Pr}$  has been studied using a 15 clover Compton-suppressed

array. Some new  $\gamma$ -ray transitions have been added to the existing level scheme. Firm spin and parity assignments for levels have been made for the first time from our  $R_{\text{DCO}}$  and polarization measurements of  $\gamma$ -ray transitions. A negative-parity  $\Delta I = 1$  magnetic dipole band has been identified. The experimental results for this band have been compared with the TAC calculations. A 3qp  $\pi(h_{11/2})^1 \otimes \nu(h_{11/2})^{-2}$  and a 5qp configuration  $\pi(h_{11/2})^1(g_{7/2})^2 \otimes \nu(h_{11/2})^{-2}$  have been assigned to the band before and after band crossing on the basis of the TAC calculations. In the future, lifetime measurements for the band levels may be helpful to confirm the MR nature of band 3.

#### ACKNOWLEDGMENTS

The authors gratefully acknowledge the support provided by the Pelletron staff at IUAC, New Delhi, INGA Collaboration, and the Department of Science and Technology, India, for providing funds for the INGA project (Grant No. IR/S2/PF-03/2003-I). This work was performed under Collaborative Research Scheme No. (CRS/2009/NP02/1350) of UGC-DAE Consortium for Scientific Research. R.G. would like to acknowledge CSIR, India, for financial assistance.

- 
- [1] B. Singh, R. Zywina, and R. B. Firestone, *Nucl. Data Sheets* **97**, 241 (2002).
  - [2] S. Mukhopadhyay, D. Almehed, U. Garg, S. Frauendorf, T. Li, P. V. Madhusudhana Rao, X. Wang, S. S. Ghugre, M. P. Carpenter, S. Gros, A. Hecht, R. V. F. Janssens, F. G. Kondev, T. Lauritsen, D. Seweryniak, and S. Zhu, *Phys. Rev. Lett.* **99**, 172501 (2007).
  - [3] Amita, A. K. Jain, and B. Singh, *Table of Magnetic-Rotational Dipole (Shears) Bands*, revised edition at <http://www.nndc.bnl.gov/publications/preprints/mag-dip-rot-bands.pdf>.
  - [4] J. R. Leigh, K. Nakai, K. H. Maier, F. Pühlhofer, F. S. Stephens, and R. M. Diamond, *Nucl. Phys. A* **213**, 1 (1973).
  - [5] P. K. Weng, P. F. Hua, S. G. Li, S. X. Wen, L. H. Zhu, L. K. Zhang, G. J. Yuan, G. S. Li, P. S. Yu, C. X. Yang, X. F. Sun, Y. X. Guo, and X. G. Lei, *Phys. Rev. C* **47**, 1428 (1993).
  - [6] E. S. Paul *et al.*, *Nucl. Phys. A* **690**, 341 (2001).
  - [7] C. F. Liang, P. Paris, D. Bucurescu, and M. S. Rapaport, *Phys. Rev. C* **40**, 2796 (1989).
  - [8] T. M. Semkow, D. G. Sarantites, K. Honkanen, V. Abenante, L. A. Adler, C. Baktash, N. R. Johnson, I. Y. Lee, M. Oshima, Y. Schutz, Y. S. Chen, J. X. Saladin, C. Y. Chen, O. Dietzsch, A. J. Larabee, L. L. Riedinger, and H. C. Griffin, *Phys. Rev. C* **34**, 523 (1986).
  - [9] M. Kortelahti, R. Julin, J. Hattula, A. Pakkanen, and M. Piiparinen, *Z. Phys. A* **321**, 417 (1985).
  - [10] H. Klewe-Nebenius, D. Habs, K. Wissak, H. Faust, G. Nowicki, S. Göring, H. Rebel, G. Schatz, and M. Schwall, *Nucl. Phys. A* **240**, 137 (1975).
  - [11] E. Y. Yeoh, S. J. Zhu, J. G. Wang, Z. G. Xiao, M. Zhang, W. H. Yan, R. S. Wang, Q. Xu, X. G. Wu, C. Y. He, G. S. Li, Y. Zheng, C. B. Li, X. P. Cao, S. P. Hu, S. H. Yao, and B. B. Yu, *Phys. Rev. C* **85**, 064322 (2012).
  - [12] E. S. Paul *et al.*, *Nucl. Phys. A* **727**, 207 (2003).
  - [13] P. Agarwal, S. Kumar, S. Singh, R. K. Sinha, A. Dhal, S. Muralithar, R. P. Singh, N. Madhavan, R. Kumar, R. K. Bhowmik, S. S. Malik, S. C. Pancholi, L. Chaturvedi, H. C. Jain, and A. K. Jain, *Phys. Rev. C* **76**, 024321 (2007).
  - [14] S. Botelho, W. A. Seale, L. G. R. Emediato, J. R. B. Oliveira, M. N. Rao, R. V. Ribas, N. H. Medina, E. W. Cybulski, M. A. Rizzutto, F. R. Espinoza-Quiñones, G. García-Bermúdez, H. Somacal, and M. A. Cardona, *Phys. Rev. C* **58**, 3726 (1998).
  - [15] E. S. Paul, C. Fox, A. J. Boston, H. J. Chantler, C. J. Chiara, R. M. Clark, M. Cromaz, M. Descovich, P. Fallon, D. B. Fossan, A. A. Hecht, T. Koike, I. Y. Lee, A. O. Macchiavelli, P. J. Nolan, K. Starosta, R. Wadsworth, and I. Ragnarsson, *Phys. Rev. C* **84**, 047302 (2011).
  - [16] K. Wissak, H. Klewe-Nebenius, D. Habs, H. Faust, G. Nowicki, and H. Rebel, *Nucl. Phys. A* **247**, 59 (1975).
  - [17] A. Goswami, S. Bhattacharya, M. Saha, and S. Sen, *Phys. Rev. C* **37**, 370 (1988).
  - [18] Y. S. Chen, S. Frauendorf, and G. A. Leander, *Phys. Rev. C* **28**, 2437 (1983).
  - [19] H. Toki and A. Faessler, *Nucl. Phys. A* **253**, 231 (1975).
  - [20] J. Meyer-Ter-Vehn, *Nucl. Phys. A* **249**, 141 (1975).
  - [21] D. A. Arseniev, A. Sobczewski, and V. G. Soloviev, *Nucl. Phys. A* **126**, 15 (1969).
  - [22] J. T. Matta, U. Garg, W. Li, S. Frauendorf, A. D. Ayangeakaa, D. Patel, K. W. Schlax, R. Palit, S. Saha, J. Sethi, T. Trivedi, S. S. Ghugre, R. Raut, A. K. Sinha, R. V. F. Janssens, S. Zhu, M. P. Carpenter, T. Lauritsen, D. Seweryniak, C. J. Chiara, F. G. Kondev, D. J. Hartley, C. M. Petrache, S. Mukhopadhyay, D. V. Lakshmi, M. K. Raju, P. V. Madhusudhana Rao, S. K. Tandel, S. Ray, and F. Dönau, *Phys. Rev. Lett.* **114**, 082501 (2015).
  - [23] V. I. Dimitrov, F. Dönau, and S. Frauendorf, *Phys. Rev. C* **62**, 024315 (2000).

- [24] G. K. Mehta and A. P. Patro, *Nucl. Instrum. Methods Phys. Res. A* **268**, 334 (1988).
- [25] D. Kanjilal, S. Chopra, M. M. Narayanan, I. S. Iyer, V. Jha, R. Joshi, and S. K. Datta, *Nucl. Instrum. Methods Phys. Res. A* **328**, 97 (1993).
- [26] S. Muralithar *et al.*, *Nucl. Instrum. Methods Phys. Res. A* **622**, 281 (2010).
- [27] S. Muralithar *et al.*, *J. Phys.: Conf. Ser.* **312**, 052015 (2011).
- [28] B. P. Ajith Kumar, E. T. Subramaniam, K. Rani, and K. Singh, in *Proceedings of DAE-BRNS Symposium on Nuclear Physics*, edited by Arun K. Jain and D. C. Biswas (Saha Institute of Nuclear Physics, Kolkata, India, 2001), Vol. 44B, p. 390.
- [29] R. K. Bhowmik, S. Muralithar, and R. P. Singh, Proc. DAE-BRNS Symp. Nucl. Phys. **B44**, 422 (2001).
- [30] D. C. Radford, *Nucl. Instrum. Methods Phys. Res. A* **361**, 297 (1995).
- [31] K. Starosta *et al.*, *Nucl. Instrum. Methods Phys. Res. A* **423**, 16 (1999).
- [32] R. Palit, H. C. Jain, P. K. Joshi, S. Nagaraj, B. V. T. Rao, S. N. Chintalapudi, and S. S. Ghugre, *Pramana* **54**, 347 (2000).
- [33] C. Ekström, S. Ingelman, M. Olsnats, B. Wannberg, G. Andersson, and A. Rosen, *Nucl. Phys. A* **196**, 178 (1972).
- [34] T. W. Conlon, *Nucl. Phys. A* **213**, 445 (1973).